Experimental and theoretical investigation of 2D nanoplatelet-based conversion layers for color LED microdisplays

E. Quesnel, A. Suhm, M. Consonni, M. Reymermier, G. Lorin, C. Laugier, M. Tournaire, P. Le Maitre, A. Lagrange, B. Racine, et al.

European Commission

Document Title	Experimental and theoretical investigation of 2D nanoplatelet-based conversion layers for color LED microdisplays.
Authors	*E. Quesnel[1]*, A. Suhm[1], M. Consonni[1], M. Reymermier[1], G. Lorin[2], C. Laugier[1], M. Tournaire[1], P. Le Maitre[1], A. Lagrange[1], B. Racine[1], M. D'Amico[3], E. Cao[3].* [1] Université Grenoble-Alpes, CEA, LETI, MINATEC Campus, 17 rue des Martyrs, F-38054 Grenoble cedex, France. [2] Université Grenoble-Alpes, CEA, LITEN, MINATEC Campus, 17 rue des Martyrs, F-38054 Grenoble cedex, France. [3] NEXDOT, 102 avenue Gaston Roussel Biotech-bâtiment Pasteur, 93230, Romainville, France.
Issue date	June 21, 2021
Journal	Optics Express
Doi	https://doi.org/10.1364/OE.425907
Acknowledgment	This project has received funding from the Clean Sky 2 Joint Undertaking under the European Union's Horizon 2020 research and innovation programme under grant agreement No 755497.
Disclaimer	The content of this article reflects only the author's view. The Clean Sky Joint Undertaking is not responsible for any use that may be made of the information it contains.

Experimental and theoretical investigation of 2D nanoplatelet-based conversion layers for color LED microdisplays.

E. QUESNEL[1]*, A. SUHM[1], M. CONSONNI[1], M. REYMERMIER[1], G. LORIN[2], C. LAUGIER[1], M. TOURNAIRE[1], P. LE MAITRE[1], A. LAGRANGE[1], B. RACINE [1], M. D'AMICO[3], E. CAO[3].

[1] *Université Grenoble-Alpes, CEA, LETI, MINATEC Campus, 17 rue des Martyrs, F-38054 Grenoble cedex, France.*

[2] *Université Grenoble-Alpes, CEA, LITEN, MINATEC Campus, 17 rue des Martyrs, F-38054 Grenoble cedex, France.*

[3] *NEXDOT, 102 avenue Gaston Roussel Biotech-bâtiment Pasteur, 93230, Romainville, France.*

* etienne.quesnel@cea.fr

Abstract: In the field of augmented reality, there is a need for very bright color microdisplays to meet the user specifications. Today, one of the most promising technology to manufacture such displays involves a blue micro-LED technology and quantum dots-based color conversion layers. Despite recent progress, the external power conversion efficiencies (EPCE) of these layers remain under ~25%, below the needs (>40%) to reach a white luminance of 100,000 cd/m^2. In this work, we have synthesized $CdSe_xS_{1-x}$ nanoplatelet-based conversion layers for red and green conversion, and measured their absorption properties and EPCE performances with respect to layer thickness. On this basis, a model was developed that reliably predicts the layer EPCE while using only few input data, namely the layer absorption coefficients and the photoluminescence quantum yield (PLQY) of color photoresist. It brings a new insight into the conversion process at play at a micro-LED level and provides a simple method for extensive optimization of conversion materials. Finally, this study highlights the outstanding red conversion efficiency of photoresist layers made of core-double shell $CdSe_xS_{1-x}$ nanoplatelets with 31% EPCE (45% external PLQY) for 8 µm-thick conversion layer.

1. Introduction

Today, the microdisplay market is dominated by projector and camera (viewfinder) applications. In the future, it could be driven by Augmented Reality (AR) applications with an increasing demand for full-color microdisplays in Head Mounted Display (HMD) and Head Up Display (HUD) systems. However, this new market needs increasingly bright displays exceeding current commercial microdisplay performances. Depending on the field of application (smart glass [1], health [2], avionics [3]) the expected microdisplay brightness can range from 10 to several 100 of kcd/m^2 [4]. Among available display technologies, best performing OLED (Organic Light Emitting Device) commercial products can reach over 20,000 cd/m² for monochrome, and over 3,000 cd/m ^{2} for high contrast bi-color microdisplays [1] with recent evolutions toward a full color brightness of 10,000 cd/m². In the same manner, full color micro-Liquid Cristal Displays (LCD) have been recently reported with at least 34,000 cd/m^2 [5] but the known downsides of a poor black level and low power efficiency.

To ensure high brightness and contrast together with better power efficiency, the micro-LED displays are viewed as one of the most promising emerging solutions and has gained considerable attraction in recent years [6, 7]. The manufacturing of very bright monochrome microdisplay prototypes has been demonstrated recently with brightness up to 3 million cd/m^2 in green [8]. However, there is still a lack of high luminance full color microdisplay demonstrators based on this technology.

Today, the best solution for building an RGB LED microdisplay is to start from an array of blue emitting pixels directly transferred and bonded to a silicon-based driving integrated circuit (IC) and partially covered with blue-to-green and blue-to-red optical converters. These converters are generally photoresist layers integrating photo-luminescent nano-semiconductors known as quantum dots (QD). There are several works investigating the integration of QD-based conversion layers into LED or OLED displays [7, 9-20]. They provide particularly interesting data on the capability of manufacturing RGB LED or OLED microdisplays. However, to our knowledge, only a few of them provide measured color conversion efficiency data that can be used to assess the performance of QD-based color conversion technology. In table I, we have listed these published data, focusing on the external power conversion efficiencies (EPCE) to provide a comparative state of the art. On a display point of view, it is indeed more relevant to assess the EPCE parameters than the usual photoluminescence quantum yield characteristics (PLQY) as often highlighted. The EPCE value enables a straightforward calculation of color light radiant power (and equivalent luminance) that a display could produce knowing the blue radiant power generated by its pixel array.

The EPCE parameter is actually linked to the external photoluminescence quantum yield (EPLQY) by the following relation:

$$\text{EPCE} = \frac{P_c}{P_b} = \text{EPLQY}\,\frac{\lambda_b}{\lambda_c} \tag{1}$$

Table 1. Comparison of literature conversion data.

Material	CNM[a] (wt%)	λ_c[a] (nm)	t[a] (μm)	EPCE[a] (%)	LED Architecture	Comment	Ref.
CdSe/ZnS QD in EOC130 PR	~4.5	540	10	6.8	40x40 μm^2 blue LED pixels	includes CF filter and glass cover	[14]
	~3.5	650	1	2			
	''	''	5	3.5			
	''	''	10	10			
CdSe/ZnS QD in EOC130 PR	3.5	630	2	22.7	ϕ320 μm blue LED	EPCE measured under λ_{blue} = 440 nm	[15]
PbBr$_3$ QD in PR	~15	528	9.8	8.2	100 x 200 μm^2 blue LED pixels	Calculated from EPLQY given in ref. (λ_{blue} = 452 nm)	[13]
CdSe QD in PR	''	636	6	3.2			
CdSe QDs		535	3.8	10.8	35 x 35 μm^2 UV LED pixels	EPCE measured under λ_{UV} = 395 nm.	[17]
		630	3.8	6.9			
CdSe/ZnS QD in PR	15	526	10.2	6.9	~150x50 μm^2 blue OLED pixels	EPCE calculated from external LCE of ref.	[18]
	''	622	10.5	8.9			
InP/ZnS in PR	15 to 50	530	4.5	20	100x300 μm^2 blue pixels	EPCE calculated from EPLQY of ref (λ_{blue} = 450 nm).	[21, 22]
		''	7	25			
		630	4.5	24.7			
		''	8	26			
CdSe$_x$S$_{1-x}$/CdS &ZnS double shell NPLs in PR	10	535	8	6.5	1 mm^2 blue LED and 9.5μm-pitch micro-LED array	EPCE measured vs layer thickness on 1 mm^2- LED (λ_{blue} = 452 nm).	This work
	10	548	7.5	11.5			
	10	650	8	31			

[a] CNM is the proportion of conversion nano-material (QDs or NPLs) in the photoresist (PR), λ_c the wavelength of emitted color light, t the conversion layer thickness and EPCE the external power conversion efficiency. LED architecture is the structure on which the conversion layers were deposited either by ink-jet or spin-coating technology.

In this expression, EPLQY is the ratio between the number of color photons emitted and the number of blue photons irradiating the conversion layer. P_c and P_b are the radiant power of emitted converted color light and the total irradiating blue light, respectively. λ_b and λ_c are the peak wavelengths of blue pumping and color converted light, respectively.

In the same manner, the internal power conversion efficiency (IPCE) can be expressed as:

$$IPCE = \frac{P_c}{P_b^{abs}} = PLQY \frac{\lambda_b}{\lambda_c} \tag{2}$$

where P_b^{abs} is the radiant power of absorbed blue excitation light and PLQY the ratio between the number of color photons emitted and the number of absorbed blue photons.

The EPCE values reported in table I were not always directly available from publications; some of them have been thus calculated from the conversion efficiencies given in the reference papers. Most conversion efficiencies were measured with ~450 nm blue light excitation, some with shorter blue or UV wavelengths. Most conversion layers are made of Cd-based QDs dispersed in a photoresist (PR). Other conversion data, available in the open literature and dealing with Cd-free nano-converters are also reported [21, 22]. The conversion performances measured in the present work are also given for comparison.

We observe a high disparity in EPCE values which obviously depend on the conversion material and the conversion layer thickness. The best blue-to-red EPCE reaches ~22% with CdSe QDs and a 440 nm blue pump. Up to 27% is claimed in ref. [22] with high concentration InP-based QDs for a 10 µm-thick layer, maximum thickness compatible with most micro-display technologies (limitation in pixel height-lateral size ratio). For blue-to-green conversion, it is almost 11% with CdSe QDs and 26% with high concentration InP-based QDs.

To assess the relevance of these values for high brightness RGB microdisplay, we must come back to the application specifications. A recent publication shows that for outdoor environment, the required luminance should exceed 10 kcd/m^2 [4]. Actually, 50 to 100 kcd/m^2 is probably more adapted to most optical combiners used so far in the available AR systems. In a previous paper [3], we have estimated the color conversion efficiency required for AR microdisplay applications. We considered a blue 9.5 µm-pitch micro-LED array exhibiting 8 or 15% electroluminescence efficiency (EL), a CMOS display driver delivering 2.6 W electric power, and a requirement of at least 20% of lit on pixels to enable video mode operation. In these conditions and with a more realistic EL value of 4.5%, the minimum EPCE values to reach for instance 100.000 cd/m^2 is around 50% and 40% for green and red conversion, respectively (Note S1 in Supplemental Document). Looking to Table 1, this target appears quite challenging, hence requiring further development of alternative conversion layers and accurate evaluation methodologies to check if such EPCE targets are actually reachable.

This is precisely the objective of this work where we propose a methodology based on coupled experimental and theoretical approaches to assess thoroughly the conversion layer performances. We will show that a spectrophotometric characterization of conversion layers associated with a dedicated light conversion model can give access to EPCE (IPCE) characteristics with an accuracy of ~±10%. It should enable an easier screening of conversion layers of various compositions without implementing complex integration technologies on micro-LED arrays. Furthermore, to validate this approach, the material investigated in this study involves two-dimensional nano-converters, namely core/double shell CdSe$_x$S$_{1-x}$ -based nanoplatelets (NPLs) instead of more conventional QDs. We will see that this kind of nanomaterials exhibits interesting efficiencies for high luminance display applications.

2. Material and methods

The experiments implemented in this study involved (i) color photoresist preparation, (ii) conversion layer deposition on glass substrates for optical characterization and (iii) layer conversion efficiency measurements under blue light excitation. The goal was to extract the main optical parameters to be used in the color conversion model and to compare the model outputs with experimental data.

2.1 Color photoresist ink preparation

The preparation of negative color conversion photoresist was carried out at NEXDOT Company. It involved the synthesis of $CdSe_xS_{1-x}$ -based core-shell nanoplatelets on the basis of seminal work done by Dubertret et al [23]. For both green- and red-emitting NPLs, we chose to focus on core/multi-shell structures, since they present better stability in time and under blue photon flux than single shell structures [3]. The general composition of red and green NPLs was a $CdSe_xS_{1-x}$-based 2D-core covered with ZnS &CdS-based double shell. This composition (x) was tuned to induce efficient emission in red and green. Moreover, the surface chemistry of NPLs was engineered with dedicated ligands [24, 25] to minimize non-radiative recombination and ensure their stability in the photoresist solution. The final synthesis of various color photoresists was achieved by mixing the NPLs with TiO_2 light scattering nanoparticles in a commercial negative polymer photoresist (POLYRISE Company [26]) and ethanol as solvent. In such photoresist, the typical concentrations of both NPLs and TiO_2 nanoparticles were ≤10 wt%. The benefit expected from these scattering TiO_2 nanoparticles is an enhanced light conversion efficiency [27]

Several batches of red and green photoresists were thus prepared for color conversion efficiency assessment. They emit either in red (λ_c = 650 nm) or in green (λ_c = 548 and 534 nm, respectively). The shorter green emission wavelength could be indeed better suited to enhance the color gamut of future RGB micro-LED displays.

A preliminary absolute measurement of resist photoluminescence quantum yield was systematically performed both on dilute photoresist solution (10 nM NPL in resin formulation into 3 mL of ethanol) and on very thin spin-coated and cured films (<0.5 µm) using a Hamamatsu equipment (Quantaurus-QY® C11347-12 spectrometer). In these conditions, the reabsorption phenomena of PL signal is very low and we can consider that the quantum yield thus measured corresponds to the intrinsic quantum yield of NPLs once embedded in the photo-polymer environment. In the following, this value is referred as QY to avoid confusion with the PLQY of the conversion layer.

2.2 Optical characterization of conversion layers

As listed in table 2, two kinds of conversion layers were investigated that were deposited by spin coating on standard glass slides for optical characterization.

Set #1 of layers was first prepared to optimize the photoresist composition, in particular the optimum TiO_2 loading. These coatings were deposited by spin coating at high spinning rate and UV cured using a laboratory UV lamp at ~100 mJ/cm².

Set #2 comprises thicker photo-patterned conversion layers which were prepared exactly in the same conditions as the conversion layers used for the EPCE measurements. These coatings were UV cured with a typical dose of 200 mJ/cm² using a microelectronics photolithography tool (SÜSS MicroTech MA8 equipment). The objective was to determine the absorption coefficient spectral dispersion ($\alpha(\lambda)$) of the three different colored photoresists in the visible range, these data being necessary to simulate the light conversion PCE dependence with layer thickness.

For both sample sets, the layer thickness was systematically measured by mechanical profilometry. Since the conversion layers contain TiO_2 nanoparticles to enhance the blue light

trapping, they obviously exhibit rather high optical scattering. That is why we measured their total transmittance (TT) and reflectance (TR) using a spectrophotometer (Lambda 950 tool from Perkin Elmer) equipped with an integrated sphere to collect the light transmitted and reflected in the whole space.

Table 2. Conversion layers investigated: photoresist (PR) characteristics and layer processing conditions

Type of layer	t^* (µm)	NPLs (wt%)	TiO_2 (wt%))	Spinning** rate (rpm)	UV curing (source : dose (mJ/cm^2)	Objective
#1 Thin layers	0.5-1	1-10	0-10	2000	Hg Lamp : 100	Best PR formulation
#2 Thick layers	3-7	10	5	500-1000	Hg Lamp : 200	Absorption of PR used in EPCE meas[rt]

*t: layer thickness; ** spin-coating deposition

In the wavelength range of interest (400 nm-λ_c), the level of measured optical losses (OL = 1-TT-RT) is rather high (see section 4). We then assume that the layers behave as a quasi-purely absorbing medium, so the optical losses are dominated by light absorption (OL~A). Hence, the blue and converted light attenuation in the conversion layer can be calculated using a simple exponential attenuation law. The radiant power p of light of wavelength λ passing through a layer of thickness t is then:

$$p(t, \lambda) = p_0(\lambda) . e^{-\alpha(\lambda).t} = [1 - A(\lambda)]. p_0(\lambda)$$

Which gives for the absorption coefficient:

$$\alpha(\lambda) = -\frac{1}{t}\ln[1 - A(\lambda)] \tag{3}$$

$A(\lambda)$ is the absorption measured at each wavelength ($A(\lambda)=1-TT(\lambda)-RT(\lambda)$). It is measured with good accuracy ($\pm 1\%$); so relative error on α results mainly on thickness (t) measurement error and is estimated to be $\pm 10\%$.

2.3 EPCE and IPCE measurements

The conversion efficiencies of several green and red conversion layers and their layer thickness dependence were measured using the experimental set-up of Fig. 1a. The light radiant power emitted by the LED covered with the conversion layer was measured in a 2π sr solid angle using an integrated sphere equipped with a calibrated spectro-radiometer. The conversion layers were deposited on the sapphire cover plate of 1 mm^2-LEDs (LUXEON Z LXZ1-PR01 from Lumileds, see inset of Fig. 1) using the same procedure as for the layers of set #2. The layer thickness was tuned by changing the spinning rate (500-1000 rpm range) or by double spin-coating. For each LED sample, the conversion layer thickness was deduced from measured absorbed blue radiant power (P_b^{abs}) using the absorption coefficient α(452 nm) and equation (4) (see next section). The accuracy on P_b^{abs} measurement is good ($< \pm 2$ %), so the thickness accuracy depends mainly on error on α and is estimated to be ± 12 %.

Each LED was calibrated prior to coating deposition so that the exact blue radiant power P_b exiting the sapphire cover plate of LED and pumping the conversion layer was perfectly known. A Peltier module was used to regulate the LED temperature at 25 °C on the rear face of its PCB. Except if otherwise mentioned, the blue light radiant power irradiating the conversion layer was fixed at 0.75W/cm^2. This value is representative of microdisplay pixel working conditions for a mean white luminance of ~100.000 cd/m^2 [3]. A typical emitted power spectrum of a LED device covered with a red conversion layer is given in Fig. 1b. The P_c radiant power is calculated by integrating the spectrum $p_c(\lambda)$ of red emission (red area). The blue peak at 452 nm is the residual blue light component which has not been absorbed by the conversion layer and is used to calculate the absorbed blue radiant power (P_b^{abs}). For instance, in the example of

Fig. 1b, the radiant power of non-absorbed blue light and emitted red light are calculated to be 0.26 and 2.1 mW, respectively for an initial blue radiant power of 7.5 mW. Both power conversion parameters are thus EPCE = 2.1/7.5 and IPCE = 2.1/(7.5-0.26), namely 28% and 29%, respectively.
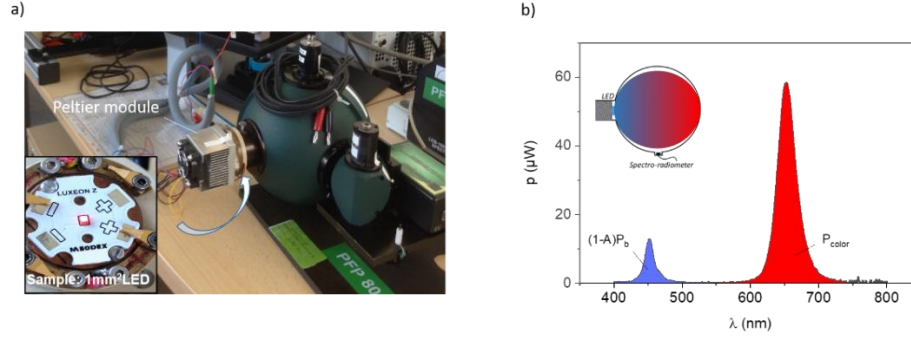

Fig. 1. (a) Optical test bench used to measure the converted light and typical LED covered with a red conversion layer mounted on its star-like PCB (insert). (b) Example of emitted power spectrum measured on a blue LED covered with a red conversion layer. The spectrum that peaks at 452 nm is the spectrum of non-absorbed blue light. Those with a peak at 650 nm is the spectrum of red emitted light resulting from the conversion of absorbed blue light.

3. Model

To better understand the light conversion mechanisms in $CdSe_xS_{1-x}$ NPL-based conversion layers, we built an optical model. The goal was to predict the EPCE thickness dependence of a NPL-based conversion layer knowing only three parameters: its QY factor and its absorption coefficients at blue peak (α_b) and color peak (α_c) wavelength. The validity of the model will be discussed in the next section by comparison with experimental conversion data.

The blue LED covered with its conversion layer and used for our conversion measurements can be depicted as the sketch of Fig. 2. Apart from the sapphire cover plate inserted between LED and conversion layer, it is very similar to the architecture of a color pixel in a microdisplay. Based on this device architecture, a modelling approach has been built considering various simplifying assumptions.

• The optical coupling between LED/sapphire and conversion layer is assumed to be optimal with 100% of blue radiant power P_b (exiting the sapphire) transferred to the conversion layer. The conversion layers are mainly composed of a polymer matrix. Their refractive index is hence around 1.6, value very close to the refractive index of sapphire (n = 1.77), avoiding significant reflection at sapphire-conversion layer interface. Note that in a real pixel configuration on a display, the optical coupling between the micro-LED pixel (n_{GaN} = 2.5) and the conversion layer would be a little less favorable with ~96% blue light transferred to the conversion layer.

• The mean light extraction efficiency (LEE) is taken equal to 95% for both colors. These values result from the refractive index mismatch between air and conversion layer assuming a layer mean refractive index of 1.6.

• The conversion layer is considered as a purely absorbing medium as shown by spectrophotometry measurements. For a given propagation light path x, the light intensity decay is then equal to I(x) = I(0) exp(-αx) where α is the mean absorption coefficient.

• Only forward propagation of blue and color light is considered. For the blue light which passes through the whole conversion layer, this assertion consists in neglecting the back-reflection of non-absorbed blue light reaching the conversion layer-air interface. Since

maximum reflectance is 5%, this back-reflected light actually represents very little blue light power. However, it must be noted that the blue light back-reflected by the TiO$_2$ scattering particles inside the coating is well taken into account in the measurement of absorption coefficient. For the emitted light, unlike the blue light, it is generated everywhere throughout the layer thickness with a part of it emitted forward and another part backward. An accurate description of the actual light propagation is difficult in such complex scattering layer structure despite first promising works done recently on that topic [28]. By considering only forward color light propagation, the risk is to slightly minimize the color light reabsorption by underestimating the color light propagation path. However, we will see that this assumption does not affect the validity of the model.
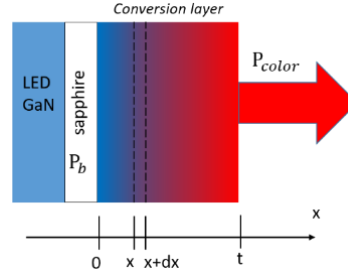

Fig. 2.Sketch of LED used for light conversion measurements. P$_b$ is the blue radiant power exiting from the sapphire cover plate and irradiating the conversion layer. P$_c$ is the converted light emitted by the conversion layer and t is the total thickness of conversion layer.

Based on these assumptions and the sketch of Fig. 2, we can calculate the EPCE and IPCE characteristics of a conversion layer. Both factors depend first on the capacity the conversion layer has to absorb the blue excitation light. The absorbed blue radiant light power can be expressed as:

$$P_b^{abs}(x) = P_b - \int_{\text{blue spect.}} p_b(\lambda)e^{-[\alpha(\lambda).x]}.d\lambda \sim P_b(1 - e^{-\alpha_b\,x}) \qquad (4)$$

Where x is the conversion layer thickness and $\alpha_b = \alpha(\lambda_b)$ the absorption coefficient at the blue peak wavelength ($\lambda_b = 452$ nm). This simplified expression of $P_b^{abs}(x)$ induces a very negligible error (<1%).

Similar approximation can be done for the attenuation of photoluminescence color light and we can write: $P_c^{attenuated} = \int_{\text{color spect.}} p_c(\lambda)e^{-[\alpha(\lambda).x]}.d\lambda \sim P_c.e^{-\alpha_c\,x}$, with $\alpha_c = \alpha(\lambda_c)$. Doing so tends to slightly underestimate the absorbed color light. It depends actually on the variation of α_c within the emission spectral range (Fig. 5). The error induced for red emission is only -1% and a little more, -10%, for green.

Now, to take into account the generation of converted light throughout the layer thickness, we consider an elementary slice of conversion layer of thickness "dx", located at x-position (Fig. 2). The blue radiant power dP$_b$ absorbed by this elementary slice of conversion layer can be expressed as:

$$dP_b = P_b.\frac{d}{dx}(1 - e^{-\alpha_b x}).$$

It will generate photoluminescence radiant power dP$_c$ that will be attenuated by absorption along the t-x distance before exiting LED device:

$$dP_c = LEE.QY.\frac{\lambda_b}{\lambda_c}.dP_b\ e^{-\alpha_c(t-x)}$$

Summing on the whole layer thickness t gives the total radiant power of emitted color light:

$$P_c(t) = LEE.QY.\frac{\lambda_b}{\lambda_c}.\int_0^t (P_b.\frac{d}{dx}(1 - e^{-\alpha_b x}).e^{-\alpha_c(t-x)}).dx$$

$$= \text{LEE} \cdot \text{QY} \cdot \frac{\lambda_b}{\lambda_c} \cdot P_b \cdot \frac{\alpha_b}{\alpha_b - \alpha_c} \cdot (e^{-\alpha_c t} - e^{-\alpha_b t})$$

Hence, the EPCE depends on layer thickness according to the following dependence equation:

$$\text{EPCE}(t) = \frac{P_c}{P_b}(t) = \text{LEE} \cdot \text{QY} \cdot \frac{\lambda_b}{\lambda_c} \cdot \frac{\alpha_b}{\alpha_b - \alpha_c} \cdot (e^{-\alpha_c t} - e^{-\alpha_b t}) \qquad (5)$$

As a result, EPCE is maximal for the given layer thickness:

$$t_{max} = \frac{1}{\alpha_c - \alpha_b} \ln\left(\frac{\alpha_c}{\alpha_b}\right) \qquad (6)$$

In the same manner, IPCE can be deduced from (5) and absorbed blue light expression P_b^{abs}. We have:

$$\text{IPCE}(t) = \frac{P_c}{P_b^{abs}}(t) = \text{LEE} \cdot \text{QY} \frac{\lambda_b}{\lambda_c} \cdot \frac{\alpha_b}{\alpha_b - \alpha_c} \cdot \frac{[e^{-\alpha_c t} - e^{-\alpha_b t}]}{(1 - e^{-\alpha_b t})} \qquad (7)$$

So, to get a first insight into the simulated conversion efficiency thickness dependence with respect to the main layer characteristics (QY, α_b and α_c), we have plotted in Fig. 3 the EPCE(t) and IPCE(t) functions. We observe that, in general, the IPCE curve shows a smooth decay with increasing thickness while the EPCE curve exhibits an optimum at a given t_{max} thickness. As expected, increasing QY increases linearly both IPCE and EPCE values (Fig. 3a). Rising α_c (Fig. 3b) has both effects, a more pronounced IPCE versus thickness decay at high t values and a slower EPCE rising slope at low t values. Moreover, higher α_c notably reduces the maximum reachable EPCE. In the same manner, increasing the blue absorption α_b (Fig. 3c) tends to increase the maximum achievable EPCE but mostly reduces the layer thickness necessary to reach this maximum. This is of utmost importance when considering the integration of conversion layer into a microdisplay. Because of pixel size aspect ratio and control of light angular emission, the layer thickness may not exceed the lateral pixel size. From this first assessment, it is clear that the ideal conversion layer should exhibit the highest α_b while keeping α_c as low as possible.
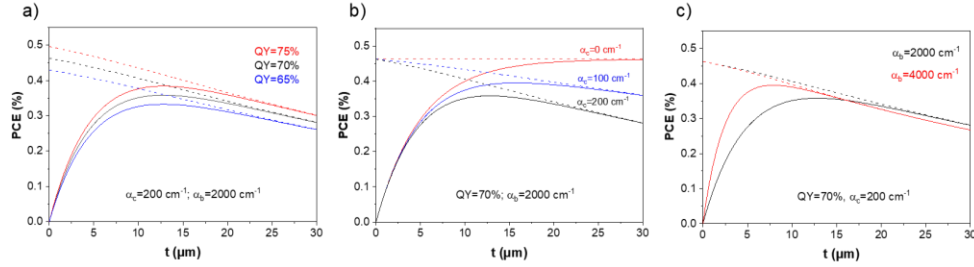

Fig. 3. Impact of model parameters on the IPCE (dashed lines) and EPCE (solid lines) functions: (a) QY, (b) α_c .and (c) α_b .The wavelengths of excitation and emission are $\lambda_b = 452$ nm and $\lambda_c = 650$ nm.

4. Results and discussion

4.1 *Optimization of photoresist composition*

Different color conversion photoresists were developed, two greens and one red. They differ from each other by their peak emission wavelength, which is adjusted by changing the composition of $CdSe_xS_{1-x}$ NPLs. For each emission color, several photoresists were prepared by mixing various loadings of NPLs and TiO_2 scattering nanoparticles (mean diameter ~30 nm) in the commercial photopolymer. The objective was to enhance as much as possible the blue light absorption and light conversion efficiency while keeping the photoresist chemically stable.

Fig. 4 illustrates the effect of both NPLs and TiO_2 loadings on the absorption coefficient spectrum of red conversion layers (samples of set #1). An optimal photoresist composition

(referred as "standard PR" in the graphs) was evidenced based on 10 wt% NPLs and 5 wt% TiO_2 loadings. Fig. 4a shows the total transmittance (TT: upper curves) and reflectance (TR: bottom curves) spectra of a 0.5 µm-thick conversion layer obtained with such standard photoresist. For comparison the response of the bare photopolymer is also given. Despite its very low thickness, this red conversion layer behaves as a very efficient absorber in the 400-650 nm range. The OL spectrum given in Fig. 4b shows two distinct absorption peaks (spotted by black arrows in the graph), which are attributed to the electron-light hole (LH) and heavy hole (HH) transitions, respectively, characteristic of colloidal CdSe-based NPL absorption spectrum [23, 29]. The optical losses are hence dominated by pure NPLs absorption (OL~A), but slight residual losses are still observable beyond the absorption threshold. They can be attributed for one part to the polymer matrix absorption and for another part to some light trapping into the substrate (light guiding effect induced by layer optical scattering).

From the OL curves measured on layers made of various photoresist compositions (not shown here), we have calculated the layer absorption coefficient spectra (Fig. 4c) using equation (3). The shape of $\alpha(\lambda)$ curves is remarkable with high blue/red absorption ratio (≥ 11) for all photoresist compositions. Moreover, these data provide an interesting insight into the role of TiO_2 scattering nanoparticles with, in particular, the evolution of the absorption coefficient with TiO_2 content (Fig. 4d). As expected, the increase of NPLs concentration enhances the layer absorption. Similarly, introduction of increasing contents of TiO_2 into the color resist significantly enhances the blue light absorption by almost 30% at the optimum TiO_2 content. However, beyond this value, further TiO_2 loading seems to mitigate the blue light absorption. Similar behavior was recently observed with a PL enhancement saturation with increasing content of $BaTiO_3$ scattering nanoparticles [27]. In our case, excess of TiO_2 probably degrades the optical coupling between incoming pumping blue light and NPLs. Moreover, the higher blue absorption induced by TiO_2 nanoparticles is systematically associated with higher reabsorption of converted light ($\alpha_b/\alpha_c = 12$ nearly constant). At maximum TiO_2 content this ratio is even degrading in favor of more reabsorption ($\alpha_b/\alpha_c = 11$).
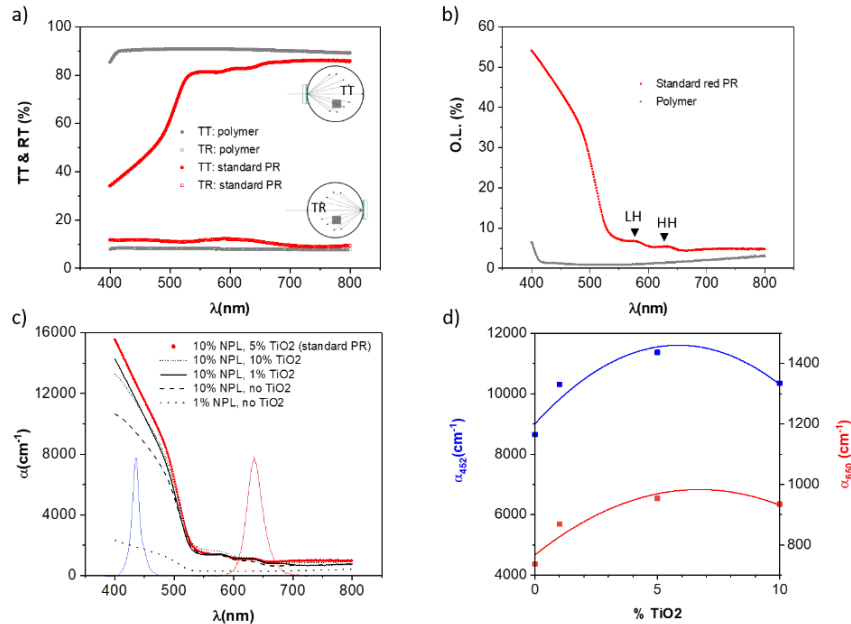

Fig. 4. (a) Total transmittance (TR) and reflectance (TR) of a 0.5 µm-thick "standard" red conversion layer with (b) corresponding OL spectrum; (c) absorption coefficient spectra of various red conversion layers of different compositions (added: blue LED and red NPLs emission spectrum); (d) evolution vs TiO_2 content of α_b and α_c (extracted from graph 4c).

Same photoresist optimization work was carried out as well on green photoresists with similar conclusions regarding the effect of TiO_2 nanoparticle loading (Note S2 in Supplemental Document). The interest of adding scattering nanoparticles will be further discussed in the next section, from the point of view of conversion efficiency and integration technology.

4.2 Optical characterization of photo-patterned conversion layers

Three kinds of photoresist were synthesized on the basis of optimized standard photoresist composition (set #2 of table 2), one red emitting at 650 nm and two greens emitting at 548 and 534 nm, respectively. The absorption spectral dispersion curves measured experimentally are given in Fig. 5. These coefficients were used as input data for the model.

As expected, the green conversion layers exhibit lower absorption coefficients than red ones. This is consistent with the fact that the S-rich $CdSe_xS_{1-x}$ green NPLs have a larger energy bandgap than the Se-rich $CdSe_xS_{1-x}$ red NPLs [23, 30]. We note however that the photo-patterned red conversion layers, although quite absorbing, are ~four times less absorbing than the red layers of Fig.4 (sample of set #1 with standard photoresist). This difference may be attributed to the different layer processing conditions used for set #1 and set #2 (table 2). It seems that set #2 processing conditions lead to less dense layers than set #1. Further experiments are ongoing to clarify this point.
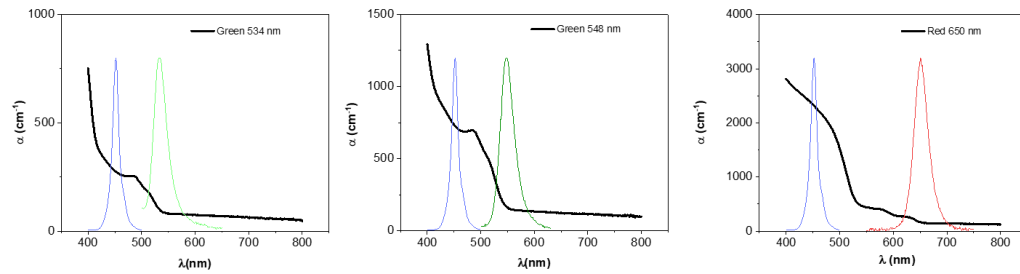

Fig. 5. Experimental absorption coefficient spectra of the 3 different types of NPL-based conversion layers (standard composition). On each graph, we have also plotted both normalized blue LED emission spectrum and conversion layer emission spectrum (peak emission wavelength: λc).

4.3 Experimental and theoretical power conversion data

To check the validity of the model, experimental EPCE and IPCE data were compared to EPCE(t) and IPCE(t) simulations for 3 conversion photoresists whose optical properties are notably different. The calculation of EPCE(t) and IPCE(t) curves have been done using equations (5) and (7) and the parameters listed in table 3. It is important to remind that α_b and α_c have been determined independently by the procedure detailed previously and were not tuned to better fit the model to the experimental data. Only the QY parameter was slightly adjusted to improve the theory-to-experience agreement. In table 3, this tuned QY parameter is compared to the initial QY^{exp} measured in solution or on very thin film. We verify that the QY values remain in the range of experimental QY^{exp} values.

Fig. 6 compares experimental and simulated data obtained for red conversion. The experimental PCE data were measured on different batches of standard NPL-based red conversion layers, which may explain that they are a little scattered. However, the agreement between experience and simulation is rather good within experimental PCE error of ± 12%. Moreover, we have also reported on graph 6b, the data extracted from literature for CdSe QD-based conversion resists. Note that the best literature data (EPCE of 22%) was obtained with a shorter 440 nm blue excitation and is probably a little overestimated with respect to our conditions of excitation

(452 nm). Anyhow, our results clearly show the superiority of red NPL-based photoresist with respect to red QD-based photoresist despite the low NPLs concentration used in our red photoresist (10 wt%).

Table 3. Experimental parameters used to calculate the EPCE (t) and IPCE(t) curves.

	λ_b (nm)	λ_c (nm)	QY^{exp} (%)	QY (%)	α_b (cm^{-1})	α_c (cm^{-1})	t_{max} [a] (µm)
Blue to red conversion	452	650	55±5%	60	2315	167	12.2
Blue to green conversion	452	548	35±5%	36	727	165	26.4
Blue to green conversion	452	534	45±5%	42	274	100	58.4

[a] We have also indicated the corresponding t_{max} values calculated using equation (6).
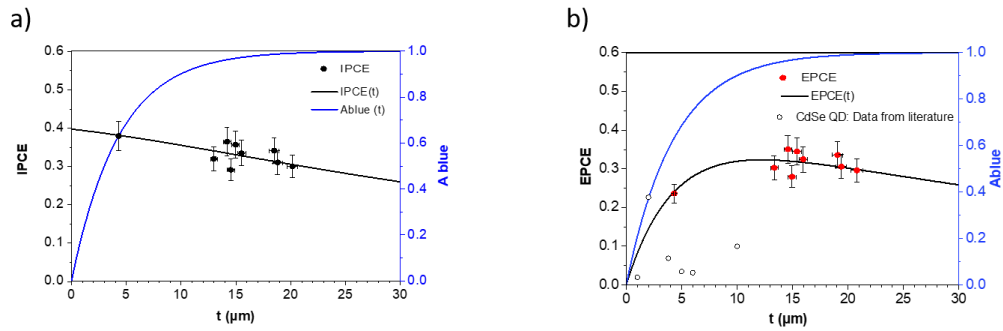

Fig. 6. Comparison of experimental (dots) and simulated (lines) blue-to-red power conversion: (a) IPCE and (b) EPCE data. The model is fitted with the parameters of table 3.The blue curve added on each graph gives the absorbed blue light calculated with equation (4). Additional EPCE literature data (o) obtained with CdSe-based red resists of table 1 are plotted for comparison.

We achieve an average of 31% EPCE at t = 13 to 16µm and predict same EPCE at ~8 µm. It is even more performing than a highly concentrated InP-based red photoresist (table 1: t = 8µm, EPCE = 26%).

As for our green conversion layers, the same theory-to-experience comparison was also performed (Fig.7). The optical properties of these layers are very different from the red ones. They show lower QY and lower absorption coefficients. Nevertheless, the model seems to fit very well with the experimental power conversion data, which tends to reinforce the reliability and consistency of our simulation approach. These green conversion layers absorb much less than the red conversion ones. Hence, a few tenths of micrometer is necessary to get significant blue absorption and conversion. This is however too thick for integration into small size pixel microdisplays. The two types of NPL-based conversion layers provide EPCE up to ~20%, but for t<10µm, they do not exceed ~13% EPCE in the best case. Comparison with published data on CdSe-based photoresists show that they achieve similar or better performances, depending on emission wavelength. However, they perform less than the highly concentrated InP QD-based green photoresist reported in table 1 (t = 7 µm, EPCE: 25%).
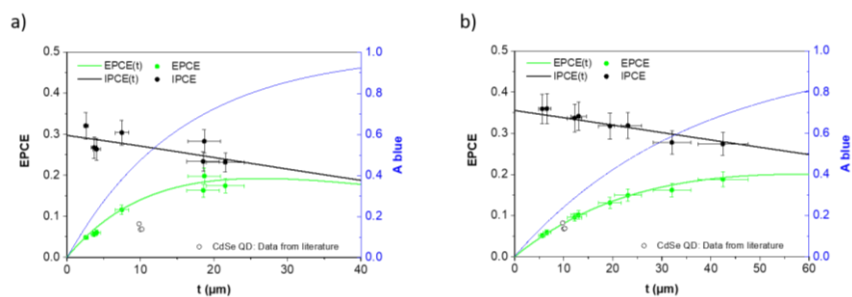
Fig. 7. Comparison of experimental (dots) and simulated (line) IPCE and EPCE results obtained with both types of green conversion layers. Emission wavelength is (a) $\lambda_c = 548$ nm and (b) $\lambda_c = 534$ nm. Additional EPCE literature data (o) obtained with CdSe-based green resists of table 1 are plotted for comparison.

4.4 Discussion

Despite a quite simple approach, the conversion model developed in this study provides a reliable estimation of EPCE conversion layer. The assumption on converted light forward propagation does not seem to significantly distort the model prediction with respect to experiment. This is probably because, in average, the absorption coefficient deduced from spectrophotometry takes more or less into account the possible back and forth light propagation induced by layer bulk scattering. The model as well as the experimental conversion data well highlight the evolution of EPCE with conversion layer thickness. The increase rate of EPCE with layer thickness was shown to depend on both blue light absorption and converted light reabsorption. As a result, maximum EPCE is reached for an optimum layer thickness (t_{max}) that not necessarily coincides with maximum blue light absorption. That means that regarding the microdisplay conversion integration strategy and in order to keep the EPCE as high as possible, it could be indeed more interesting to add a blue light stop filter [14] than thickening the conversion layer beyond t_{max}. Moreover, a too thick conversion layer could prevent complete photoresist reticulation since UV photo-patterning light might not reach the bottom of pixel.

On photoresist development point of view, this model allows predicting the power conversion efficiency on the basis of only three physical characteristics, the photoresist QY, and the layer optical coefficients α_b and α_c. That means that, in practice, the optimization of conversion photoresist composition could be done by simply using easily available characterization tools, i.e. a spectrophotometer operated in total reflectance and transmittance mode and a QY measurement tool routinely used by chemists to characterize their material in solution.

Another interesting result of this study is the outstanding conversion efficiency of the red NPL-based resin developed in this work. Despite a relatively low concentration in NPLs (10 wt%), EPCE experimental data exceeding 31% EPCE (EPLQY of 45%) were indeed measured on several micron-thick layers. To the best of our knowledge this result outperforms the current state of the art.

The results on NPL-based green resist are promising but not sufficient for microdisplay applications where pixel sizes smaller than 10 µm are targeted. That is why further NPL-based photoresist optimization need to be conducted mainly by investigating different shells to increase blue light absorption. The issue of their chemical and environmental stabilities should be also solved to further their longevity and stability with time. Furthermore, new materials like green emitting perovskite could be also an interesting alternative solution since they are known to offer strong blue absorption together with high QY.

Beyond their conversion performances, the color conversion photoresists must also be compatible with microelectronics processing, in particular with conventional photolithography

tools. That is why, on top of this work, we have tested the ability to pattern the red NPL-based photoresist proposed in this paper and ensured that these red pixels were functional. Successful co-integration of red and blue pixels was achieved on passive monolithic 1750×1150 blue micro-LED arrays (9.5 µm-pixel pitch) bonded to a silicon-based passive interconnect circuit. The red pixels were patterned at 8-inch wafer level (Fig. 8a) according to various configurations designed to display checkerboard-like or letter-like patterns, for instance. Conversion layer deposition was performed in same conditions as layers of set#2 (Table 2). Photolithography patterning was achieved with a standard PAS 5500/100D/i-Line Stepper from ASML at a dose of 200 mJ/cm^2 (Note S3 in Supplemental Document)

Fig. 8b shows examples of such lit-on patterns, with a typical emission spectrum. Emission color is actually magenta because of remaining blue light in the spectrum (4 µm-thick red conversion pixel not absorbing 100% of blue light). The color coordinates were found to be x = 0.383 and y = 0.154, which corresponds to ~40% of blue light power within the whole spectrum (Note S4 in Supplemental Document.). This is fully consistent with Fig. 6 where a 4 µm-thick red conversion layer is expected to absorb 60% of blue light. Moreover, in absence of black matrix [12], another small additional part of this blue component could also come from blue light escaping through the walls of individual red conversion pixels since the underneath blue micro-LEDs have a Lambertian emission.
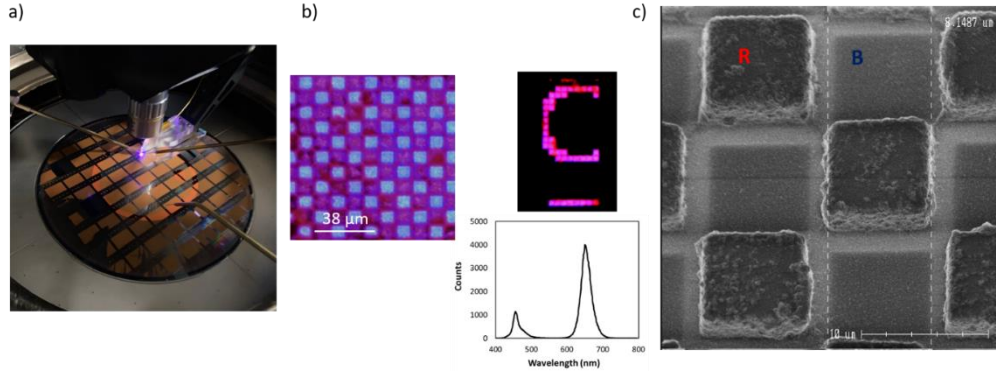

Fig. 8. (a) 8-inch wafer under test after red conversion layer pixelisation. It integrates several passive matrices of 1750×1150 pixels and additional test patterns. (b) Various lit-on patterns with typical emission spectrum. (c) Electronic microscopy image of individual 4 µm-thick 8x8 µm^2 red conversion pixels.

The morphology of the 8x8 µm^2 red pixels exhibits a nice parallelepiped shape (Fig. 8c). We observe however that the pixel top surface and walls are relatively rough with aggregation of TiO$_2$ nanoparticles. This surface roughness should facilitate light extraction. In return, it induces layer thickness non-uniformity (hence red color variation) and promotes lateral light scattering and undesirable pixel-to-pixel color crosstalk. That is why, reducing the content of scattering TiO$_2$ nanoparticles could help controlling the uniformity of pixel emission and its angular emission provided the price to pay on the conversion efficiency is not too high.

We can estimate this price using our model (Fig. 9). Figure 4d shows that suppressing the 5 wt% TiO$_2$ nanoparticles contained in the red photoresist would decrease the layer absorption (α_b and α_c) by around ~25%. As a consequence, the EPCE curve would be shifted towards higher thickness as highlighted in Fig 9. However, the maximum EPCE reachable would remain unchanged. Hence, suppressing TiO$_2$ mainly shifts the optimal layer thickness t$_{max}$ for which the EPCE is maximum. On a microdisplay point of view, a better control of pixel angular emission is a key requirement which could necessitate a drastic reduction of TiO$_2$ content. At layer thickness compatible with our pixel size (Fig. 8), for instance with a 6 µm-thick

conversion layer, suppressing TiO_2 would reduce the EPCE by around 3%, from 28 to 25%, which is not that much actually.
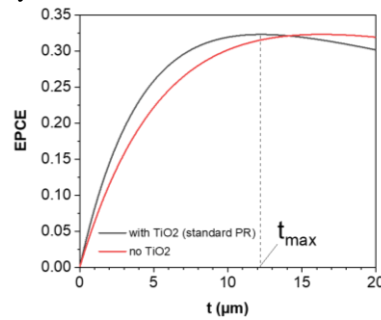

Fig. 9. (a) Evolution of EPCE (t) of red conversion layers with TiO_2 (5 wt%) and without TiO_2. Calculation was done using data of Fig. 5 and assuming -25% on absorption without TiO_2.

5. Conclusion

With the development of augmented reality market, there is an increasing demand for much brighter full color microdisplay. The micro-LED technology could be a suitable way to meet these demanding specifications. However, the existing conversion layers, generally based on color photoresists, are below the technical requirements to expect reaching 100.000 cd/m^2.

In that context, we have developed in this work a dedicated characterization and modeling approach to assess the conversion efficiency of novel conversion photoresists for red and green emission. The main outputs are:

- A model that reliably predicts the power conversion efficiency of a conversion layer while using only few of its characteristics: its absorption coefficient at light pumping and light emitting wavelengths and the photoluminescence quantum yield of initial photoresist.

- A model that brings more accurate insight into the mechanisms at play in the conversion process at a micro-LED level highlighting, for instance, the role of additional scattering nanoparticles.

- Alternative red and green light conversion photoresists based on the chemical synthesis of novel core-double shell $CdSe_xS_{1-x}$ nanoplatelets as light nano-converters. In particular, a novel red photoresist showing outstanding conversion efficiency with 31.5% EPCE value (45% external PLQY) for only 8 µm-thick conversion layer.

- First successful integration at 8 inch-wafer level of operating red pixels on monolithic 1750×1150 blue micro-LED arrays with a 9.5 µm-pixel pitch. It shows the full compatibility of photoresist with standard microelectronic tools.

These results, although promising, show that further conversion photoresist optimization are still necessary. To meet the future AR application requirements, conversion layers with at least 40% EPCE are indeed requested to reach a white luminance of 100,000 cd/m^2. The methodology proposed in this study could provide a valuable design guideline for such color photoresist optimization work.

Disclosures

The authors declare no conflicts of interest.

Data availability statement

Data underlying the results presented in this paper are not publicly available at this time but may be obtained from the authors upon reasonable request.

Supplemental document

See Supplement 1 for supporting content

References

1. G. Haas, "Microdisplays for Augmented and Virtual Reality," SID 2018 Symposium Digest of Technical Papers, p. 506, 201.
2. A. Meola, F. Cutolo, M. Carbone, F. Cagnazzo, M. Ferrari, V. Ferrari, « Augmented reality in neurosurgery: a systematic review", Neurosurg Rev (2017) 40:537–548.
3. E. Quesnel, A. Lagrange, M. Vigier, M. Consonni, M. Tournaire, V. Le Marchand, A. Suhm, P. Demars, J.-C. Pillet, B. Ben Bakir, N. Olivier, E. Feltin, J. M. Lamy, M. D'Amico, E. Cao, G. Haas, L. Charrier, P. Coni, « Dimensioning a full color LED microdisplay for augmented reality headset in a very bright environment", J Soc Inf Display. 2020; 1–14; https://doi.org/10.1002/jsid.884 .
4. T. Zhan, K. Yin, J. Xiong, Z. He, and S.-T. Wu, "Augmented Reality and Virtual Reality Displays: Perspectives and Challenges", iScience23, 101397, August 21, 2020; https://doi.org/10.1016/j.isci.2020.101397
5. https://www.displaydaily.com/article/display-daily/kopin-brillian-lcd-microdisplay-to-be-in-army-ar-hmd.
6. F. Templier, L. Dupré, B. Dupont, A. Daami, B. Aventurier, F. Henry, D. Sarrasin, S. Renet, F Berger, F. Olivier, L. Mathieu. « High-resolution, active matrix, 10-μm pixel-pitch GaN LED microdisplays for Augmented Reality applications. SPIE Proc Vol. 10556. 2018. https://doi.org/10.1117/12.2294527
7. H. Kawanishi, H. Onuma, M. Maegawa,T. Kurisu, T. Ono, S. Akase, S. Yamaguchi, N. Momotani, Y. Fujita, Y. Kondo, K. Kubota, T. Yoshida, Y. Ikawa, T. Ono, H. Higashisaka, Y. Hirano, S. Anzai, , "High-resolution and high-brightness full-colour "Silicon Display" for augmented and mixed reality", J Soc Inf Display. 2021;29: 57–67. https://doi.org/10.1002/jsid.968
8. L. Zhang, F. Ou, W.C. Chong, Y. Chen, Q. Li, "Wafer-scale monolithic hybrid integration of Si-based IC and III–V epilayers: A mass manufacturable approach for active matrix micro-LED microdisplays"; J SID. 2018; 26(3):137–145. https://doi.org/10.1002/jsid.649
9. H.-V. Han, H.-Y. Lin, C.-C. Lin, W.-C. Chong, J.-R. Li, K.-J. Chen, P. Yu, T.-M. Chen, H.-M. Chen, K.-M. Lau, and H.-C. Kuo, « Resonant-enhanced full-color emission of quantum-dot-based micro LED display technology", 14 Dec 2015 | Vol. 23, No. 25 | DOI:10.1364/OE.23.032504 | OPTICS EXPRESS 32504.
10. Z. Liu, C.-H. Lin, B.-R. Hyun, C.-W. Sher, Z. Lv, B. Luo, F. Jiang, T Wu, C.-H. Ho, H.-C. Kuo and Jr-H. He, "Review: Micro-light-emitting diodes with quantum dots in display technology", Light: Science & Applications (2020) 9:83; https://doi.org/10.1038/s41377-020-0268-1
11. Y.-M. Huang, K. J. Singh, A.-C. Liu, C.-C. Lin, Z. Chen, K. Wang, Y. Lin, Z. Liu, T. Wu, and H.-C. Kuo, "Review: Advances in Quantum-Dot-Based Displays", Nanomaterials 2020, 10, 1327; https://doi.org/10.3390/nano10071327
12. H.-M. Kim, M. Ryu, |J. H. J. Cha, H. S. Kim, T. Jeong, J. Jang, "Ten micrometer pixel, quantum dots color conversion layer for high resolution and full color active matrix micro-LED display", J Soc Inf Display. 2019;1–7, https://doi.org/10.1002/jsid.782
13. Y. Yin, Z. Hu, M. U. Ali, M. Duan, L. Gao, M. Liu, W. Peng, J. Geng, S. Pan, Y. Wu, J. Hou, J. Fan, D. Li, X. Zhang, and H. Meng, "Full-Color Micro-LED Display with CsPbBr3 Perovskite and CdSe Quantum Dots as Color Conversion Layers",Adv. Mater. Technol. 2020, 5, 2000251, https://doi.org/10.1002/admt.202000251
14. X. Zhang, L. Qi, W. C. Chong, P. Li, C. W. Tang, K. M. Lau, "Active matrix monolithic full-color microdisplay", J Soc Inf Display. 2021; 29:47–56. https://doi.org/10.1002/jsid.962
15. P. Li, X. Zhang, Y. Li, L. Qi, C.W. Tang, K.M. Lau, "Monolithic full-color microdisplay using patterned quantum dot photoresist on dual-wavelength LED epilayers", J Soc Inf Display. 2020; 1–9. https://doi.org/10.1002/jsid.966
16. S.-W. H. Chen, Y.-M. Huang, K. J. Singh, Y.-C. Hsu, F.-J. Liou, J. Song, J. CHOI, P.-T. Lee, C.-C. Lin, Z. Chen, J. Han, T. WU, and H.-C. KUO, Full-color display with high color stability using semipolar (20-21) InGaN LEDs and quantum-dot photoresist, Vol. 8, No. 5 / May 2020 / Photonics Research, https://doi.org/10.1364/PRJ.388958
17. H.-Y. Lin, C.-W. Sher, D.-H. Hsieh, X.-Y. Chen, H.-M. P. Chen, T.-M. Chen, K.-M. Lau, C.-H. Chen, C.-C. Lin, and H.-C. Kuo, "Optical cross-talk reduction in a quantum dot- based full-color micro-light-emitting-diode display by a lithographic-fabricated photoresist mold"; Vol. 5, No. 5 / October 2017 / Photonics Research; https://doi.org/10.1364/PRJ.5.000411
18. Z. Hu, Y. Yin, M.U Ali, W. Peng, S. Zhang, D Li, T Zou, Y. Li, S. Jiao, S.-J. Chen, C.-Y. Lee, H. Meng, and H. Zhou, "Inkjet printed uniform quantum dots as color conversion layers for full-color OLED displays", Nanoscale, 2020, 12, 2103; https://doi.org/10.1039/C9NR09086J
19. H.-J. Kim, M.-H. Shin, H.-G. Hong, B.-S. Song, S.-K. Kim, W.-H. Koo, J.-G. Yoon, S.-Y. Yoon and Y.-J. Kim, "Enhancement of Optical Efficiency in White OLED Display Using the Patterned Photoresist Film Dispersed

With Quantum Dot Nanocrystals", JOURNAL OF DISPLAY TECHNOLOGY, VOL. 12, NO. 6, JUNE 2016, DOI: 10.1109/JDT.2015.2503401

20. W.H. Kim, Y.J. Jang, J.-Y. Kim, M. Han, M. Kang, K. Yang, J.-H. Ryou, and M.-K. Kwon, "High-Performance Color-Converted Full-Color Arrays", Appl. Sci. 2020, 10, 2112; https://doi.org/10.3390/app10062112

21. E. Lee, S. Kan, C. Hotz, J. Yurek, Z.S. Luo, H. Kim, J. Yamanaga, A. Carpente, Ambient Processing of Quantum Dot Photoresist for Emissive Displays, SID Symposium Digest of Technical Papers. Volume 44, Issue 1, pages 984-987.

22. E. Lee, R. Tangirala, A. Smith, A. Carpenter, C. Hotz, H. Kim, J. Yurek, T. Miki, S. Yoshihara, T. Kizaki, A. Ishizuka, I. Kiyoto, "Quantum Dot Conversion Layers Through Inkjet Printing", https://www.nanosysinc.com/white-papers/2018/11/28/quantum-dot-conversion-layers-through-inkjet-printing?format=amp

23. S. Ithurria and B. Dubertret, "Quasi 2D Colloidal CdSe Platelets with Thicknesses controlled at the Atomic Level", J. AM. CHEM. SOC. 2008, 130, 16504–16505; DOI: 10.1021/ja807724e

24. A. Banerjee, C. Grazon, B. Nadal, T. Pons, Y. Krishnan, and B. Dubertret, "Fast, Efficient, and Stable Conjugation of Multiple DNA Strands on Colloidal Quantum Dots", Bioconjugate Chemistry, 2015, 26, 8, 1582–1589, https://doi.org/10.1021/acs.bioconjchem.5b00221

25. E. Giovanelli, E.Muro, G. Sitbon, M. Hanafi, T. Pons, B. Dubertret, and N. Lequeux, « Highly Enhanced Affinity of Multidentate versus Bidentate Zwitterionic Ligands for Long-Term Quantum Dot Bioimaging", Langmuir, 2012, 28, 43, 15177–15184, https://doi.org/10.1021/la302896x

26. http://www.polyrise.com/hardrise.

27. H. Yang, M. Zhou, H. Tang, M. Sun, P. Liu, Y. Liu, L. Chen, D. Li, D. Wu, J. Hao, B. Xu, Z. Zhao, Z. Ren, S. Jia, K. Wang and X. W. Sun , "Enhanced light emission of quantum dot films by scattering of poly(zinc methacrylate) coating CdZnSeS/ZnS quantum dots and high refractive index $BaTiO_3$ nanoparticles", RSC Adv., 2020, 10, 31705; https://doi.org/10.1039/D0RA05389A

28. B. Blülle, S. Altazin, B. Frouin, L. Stepanova, S. Jenatsch, B. Ruhstaller, "Light conversion and scattering properties of QD films for display applications: Angle-resolved optical spectroscopy and numerical simulation", SID 2019 DIGEST, 1720; https://doi.org/10.1002/sdtp.13285

29. J Yu, R. Chen, "Optical properties and applications of two-dimensional CdSe nanoplatelets", InfoMat. 2020; 2: 905–927, https://doi.org/10.1002/inf2.12106.

30. N. Soltani, E. Gharibshahi, E. Saion, "Band-gap of cubic and hexagonal CdS quantum dots: experimental and theoretical studies", Chalcogenide Letters Vol. 9, No. 7, July 2012, p. 321 – 328.

Experimental and theoretical investigation of 2D nanoplatelet-based conversion layers for color LED microdisplays.: supplemental document

Note S1: EPCE Specifications

In our previous work published in reference [3] we have dimensioned a full color LED microdisplay for an augmented reality application headset corresponding to a real market need. In the RRGB quad white pixel configuration described in that work and assuming 15% electroluminescence efficiency (EL), a CMOS display driver delivering 2.6 W electric power, and a requirement of at least 20% of lit on pixels to enable video mode operation, we concluded that it was possible to reach ~0.35 Mcd/m^2 maximum in video mode. This calculation assumed an EPLQY for both color conversion of 60%, which means an **EPCE of 49.5 and 41.7%** for green and red, respectively. It also assumed D65 standard white light and a maximum bias voltage of 4V at pixel level.

The table below details in column A the necessary current and voltage specifications for each pixel type to reach 1.000,000 cd/m^2. From this calculation, the maximum luminance in video mode is deduced (335.000 cd/m^2). In column B, same calculation is done with a more realistic EL value of 4.5% and same EPLQY. We can conclude that, in that case, 100.000 cd/m^2 should be reachable.

For 1,000,000 cd/m^2	A (EL 15%; EPLQY 60%)	B (EL 4.5%; EPLQY 60%)
I(μA)/V(V): Blue pixel	4.1/4	13.7/4
I(μA)/V(V): Green pixel	6.4/4	21.3/4
I(μA)/V(V): Red pixel	6.2/4	20.7/4
I(μA)/V(V): Red pixel	6.2/4	20.7/4
Power (μW): White pixel	91.7	305.6
Rate of pixel max. (%)	6.7	2
Max luminance in video mode (cd/m^2) (20% pixel max)	335,000	100,000

Note S2: Optimization of green photoresist

The green photoresist composition was optimized in the same manner as done with the red photoresist. Fig S1 shows the variation of absorption coefficient spectral dispersion for different concentrations of NPLs and TiO_2 nanoparticles. As for the red photoresist, we can observe an increase of layer absorption with NPL and TiO_2 content. Similarly, beyond ~3% TiO_2 content, the absorption tends to decrease.
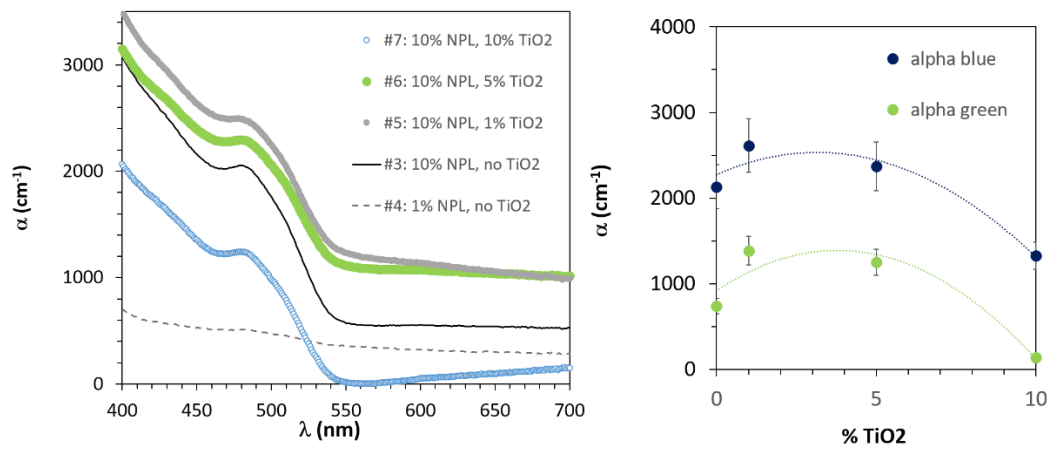
Fig. S1. (left) Variation of absorption coefficient spectral dispersion of green (534 nm) photoresist with NPL and TiO$_2$ loading. 10% NPL and 5%TiO$_2$ correspond to our standard PR formulation. (right) Evolution of blue and green absorption coefficient with TiO$_2$ content.

Note S3: MicroLED array and pixel patterning

The micro-LED arrays used for color pixel patterning tests have been processed on 1.85 x 1.85 cm^2 passive interconnect circuits (collectively manufactured on an 8-inch silicon wafer). The GaN epilayer grown on a 4-inch sapphire was directly transferred and stuck on the IC by metal-to-metal bonding and its sapphire substrate removed by laser lift-off. Then, pixelisation and electric connection were achieved. At the end, we get a smooth surface with arrays of 9.5 µm-pitch blue pixels that can be lit-on by groups of pixels (different patterns). Under 4V, the mean blue radiant power generated by the micro-LEDs is around 0.4 W/cm^2.

The color pixels are processed on top of this wafer in several steps

- PR spin-coating (1000 rpm), typically 3 ml PR ink per wafer.

- Drying at RT,

- Photolithography of pixel arrays: PAS 5500/100D/i-Line Stepper; dose: 200 mJ/cm^2

- Developing of PR using IPA (removal of un-exposed PR).

Note S4: Analysis of red pixel emission

From the typical pixel emission spectrum of Fig. 8, we have deduced the color coordinates. We found x = 0.383 and y = 0.154, which corresponds to the star point highlighted in the CIE color space chromaticity diagram of Fig S2. On this diagram, we have also indicated the color points (circle) corresponding to a bicolor light (blue + red) containing 1, 10 and 50% blue component, respectively. The star coordinates coincide with a blue-red light containing ~40% of blue light. This is fully consistent with Fig.6 where a 4 µm-thick red conversion layer is found to absorb 60% % of blue light.
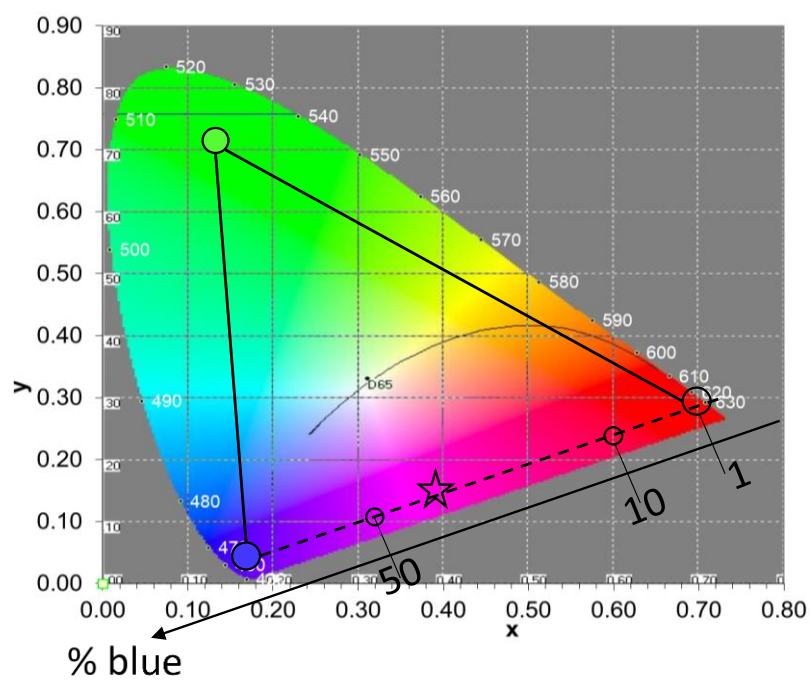
Fig. S2. Color gamut (star) of light emitted by the 4 µm-thick red-pixel of Fig.8.